4-2017

Factorization Breaking of AdT for Polarized Deuteron Targets in a Relativistic Framework

Sabine Jeschonnek

J. W. Van Orden
Old Dominion University, jvanorde@odu.edu

Original Publication Citation

Jeschonnek, S., & Van Orden, J. W. (2017). Factorization breaking of AdT for polarized deuteron targets in a relativistic framework. Physical Review C, 95(4), 044001. doi:10.1103/PhysRevC.95.044001

Factorization breaking of A_d^T for polarized deuteron targets in a relativistic framework

Sabine Jeschonnek[1] and J. W. Van Orden[2,3]
[1]*The Ohio State University, Physics Department, Lima, Ohio 45804, USA*
[2]*Department of Physics, Old Dominion University, Norfolk, Virginia 23529, USA*
[3]*Jefferson Laboratory, 12000 Jefferson Avenue, Newport News, Virginia 23606, USA*
(Received 14 June 2016; revised manuscript received 6 February 2017; published 17 April 2017)

We discuss the possible factorization of the tensor asymmetry A_d^T measured for polarized deuteron targets within a relativistic framework. We define a reduced asymmetry and find that factorization holds only in plane wave impulse approximation and if p waves are neglected. Our numerical results show a strong factorization breaking once final state interactions are included. We also compare the d-wave content of the wave functions with the size of the factored, reduced asymmetry and find that there is no systematic relationship of this quantity to the d-wave probability of the various wave functions.

DOI: 10.1103/PhysRevC.95.044001

I. INTRODUCTION

For a long time, the d-wave contribution to the deuteron has been a matter of interest. Early on, it was determined that the d wave is responsible in large part for the quadrupole moment of the deuteron. Early calculations of the deuteron wave function including the tensor force needed to produce the d-wave admixture resulted in a considerable range of values for the d state probability. Eventually it was argued that the d-wave contribution was not a physical observable [1–4].

Experimentally, there have been many measurements aimed at understanding the d wave contribution and the short range structure of the deuteron. Exclusive electron scattering from the deuteron, namely $(e,e'p)$ reactions, were initially motivated by the factorization assumption: if there are no final state interactions, the ^{2}H$(e,e'p)$ cross section would be proportional to the single-nucleon cross section multiplied with the momentum distribution $n(p)$. It has become common practice to apply some form of the factorization prescription as described by deForest [5] to measurements of the $(e,e'p)$ reaction for all nuclei. It soon became clear that the factorization assumption does not hold in general: final state interactions and other pieces of the reaction mechanism beyond the plane wave impulse approximation (PWIA) break factorization and distort the cross section. Ever since the first experiments at NIKHEF [6–11] and Saclay [12–15], the hunt has been on for kinematic regions and observables that might allow us to extract information on the deuteron's d wave [16–21]. On the theory side, considerable effort has been expended to describe the reaction mechanism, including final state interactions, meson exchange currents, isobar contributions, and either relativistic corrections or fully-fledged relativistic descriptions [22–40].

In the search for suitable observables, measurements on polarized deuteron targets have high potential. Polarization experiments have much lower count rates than their unpolarized counterparts, but they hold the promise of much more sensitive observables. The tensor asymmetry of the deuteron, accessible with an unpolarized electron beam and a tensor-polarized target, vanishes if there is no d wave. For the exclusive reaction we discuss here, one has the best prospect of disentangling information about the wave function from the reaction mechanism.

Semi-inclusive reactions on tensor-polarized deuteron have also been discussed lately, with a view to experiments at a future electron-ion collider [41–45].

One possible approach that might allow for the determination of some information about the d state would be if some region of kinematics could be found where the sensitivity to the components of the current operator and to the final state interactions is negligible. This would lead to the factorization of the polarized deuteron cross sections into an effective single nucleon part and various polarized momentum distributions. Appropriate ratios of the cross section can then be defined where the single-nucleon cross sections cancel and only a ratio of momentum distributions remains. The objective of this paper is to address the feasibility of such a process using a variety of modern high quality wave functions, a selection of single-nucleon electromagnetic form factors, and two different parametrizations of the final state interactions.

The motivation for revisiting this problem at this time is that a new polarized deuterium target is under construction to be used in Hall C at Jefferson Laboratory for the approved experiments [46] and [47]. While the first of these is for inclusive scattering to obtain the b_1 structure function for deep inelastic scattering and the second is to obtain elastic and inclusive data at kinematics that are not necessarily favorable for attempting to extract information about the deuteron d state, the existence of this target allows for the possibility of experiments more tailored to extracting this information. The practicality of such an experiment is considered here.

The paper is organized as follows. First, we briefly review the general formalism necessary to calculate response functions for polarized targets, and the definitions of the asymmetries that can be measured for polarized targets and beams. Then, we carefully discuss under which conditions the factorization of the tensor asymmetry may arise in a fully relativistic framework based on the Bethe-Salpeter equation,

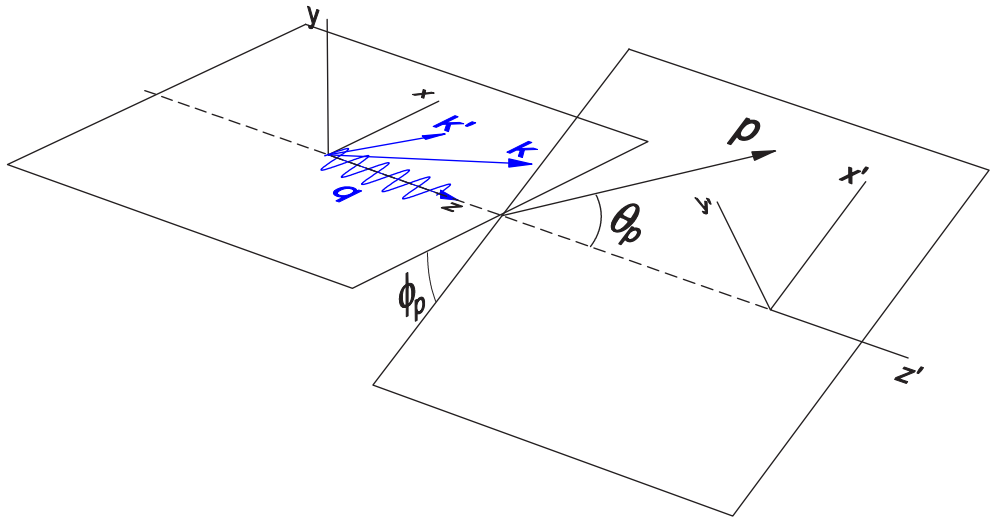

FIG. 1. Coordinate systems for the ^{2}H$(e,e'p)$ reaction. k and k' are the initial and final electron four-momenta, q is the four-momentum of the virtual photon, and p is the four-momentum of the final-state proton.

and which form the asymmetry A_d^T takes when it holds. In the next section, we present our numerical results, in a kinematic region relevant to experiments at Jefferson Lab. We show the influence of the different model inputs on the calculations. With final state interactions included, factorization breaks. We conclude with a brief summary.

II. FORMALISM

We present a brief review of the formalism for calculating the differential cross section, response functions, and asymmetries for target polarization. For a complete discussion, the reader is referred to [34].

A. Differential cross section

The standard coordinate systems used to describe the $D(e,e'p)$ reaction are shown in Fig. 1. The initial and final electron momenta $\boldsymbol{k}$ and $\boldsymbol{k'}$ define the electron scattering plane and the xyz-coordinate system is defined such that the z axis, the quantization axis, lies along the momentum of the virtual photon q with the x axis in the electron scattering plane and the y axis perpendicular to the plane. The momentum p of the outgoing proton is in general not in this plane and is located relative to the xyz system by the polar angle θ_p and the azimuthal angle ϕ_p.

The general form of the ^{2}H$(e,e'p)$ cross section can be written in the laboratory frame as [48,49]

$$\left(\frac{d\sigma^5}{d\epsilon' d\Omega_e d\Omega_p}\right)_h = \frac{m_p\, m_n\, p_p}{8\pi^3\, M_d}\,\sigma_{\rm Mott}\, f_{\rm rec}^{-1} \times [v_L R_L + v_T R_T + v_{TT} R_{TT} + v_{LT} R_{LT} + h\, v_{LT'} R_{LT'} + h\, v_{T'} R_{T'}], \quad (1)$$

where M_d, m_p, and m_n are the masses of the deuteron, proton, and neutron, $p_p = p_1$ and Ω_p are the momentum and solid angle of the ejected proton, ϵ' is the energy of the detected electron, and Ω_e is its solid angle, with $h = \pm 1$ for positive and negative electron helicity. The Mott cross section is

$$\sigma_{\rm Mott} = \left(\frac{\alpha\cos(\theta_e/2)}{2\varepsilon\sin^2(\theta_e/2)}\right)^2 \quad (2)$$

and the recoil factor is given by

$$f_{\rm rec} = \left|1 + \frac{\omega p_p - E_p q\cos\theta_p}{M_d\, p_p}\right|. \quad (3)$$

The hadronic tensor for scattering from polarized deuterons is defined as

$$W^{\mu\nu}(D) = \sum_{s_1,s_2,\lambda_d,\lambda'_d} \langle \boldsymbol{p}_1 s_1; \boldsymbol{p}_2 s_2; (-)|J^\mu|\boldsymbol{P}\lambda'_d\rangle^* \langle \boldsymbol{p}_1 s_1; \boldsymbol{p}_2 s_2; (-)|J^\nu|\boldsymbol{P}\lambda_d\rangle \rho_{\lambda_d\lambda'_d}. \quad (4)$$

The notation $(-)$ in the final state indicates that the state satisfies the boundary conditions appropriate for an "out" state. The deuteron density matrix in the xyz frame is

$$\boldsymbol{\rho} = \frac{1}{3}\begin{pmatrix} 1+\sqrt{\frac{3}{2}}\,T_{10}+\frac{1}{\sqrt{2}}T_{20} & -\sqrt{\frac{3}{2}}(T_{11}^*+T_{21}^*) & \sqrt{3}\,T_{22}^* \\ -\sqrt{\frac{3}{2}}(T_{11}+T_{21}) & 1-\sqrt{2}\,T_{20} & -\sqrt{\frac{3}{2}}(T_{11}^*-T_{21}^*) \\ \sqrt{3}\,T_{22}^* & -\sqrt{\frac{3}{2}}(T_{11}-T_{21}) & 1-\sqrt{\frac{3}{2}}\,T_{10}+\frac{1}{\sqrt{2}}T_{20} \end{pmatrix} \quad (5)$$

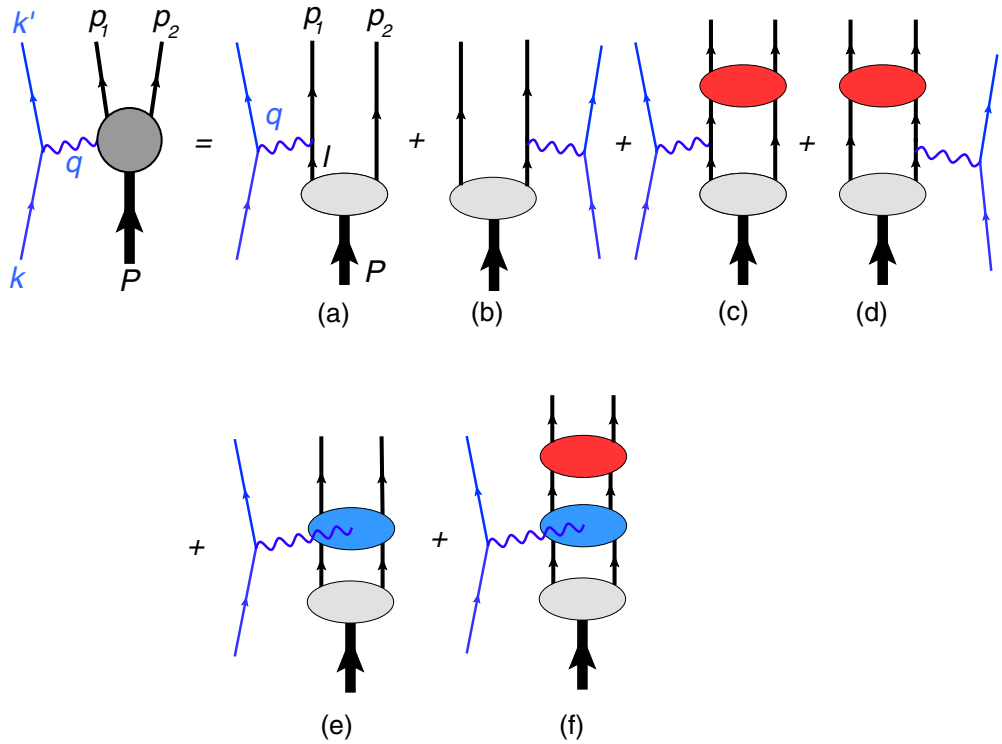

FIG. 2. Feynman diagrams for the impulse approximation.

and the set of tensor polarization coefficients is defined as

$$D = \{U, T_{10}, T_{11}, T_{20}, T_{21}, T_{22}\} \tag{6}$$

with U designating the contribution from unpolarized deuterons. The kinematic factors v_i and the polarized response functions are listed in Appendix A for convenience.

The expressions above assume that the deuteron target is polarized along the direction of the three-momentum transfer $\boldsymbol{q}$ which is defined as the z axis as defined in Fig. 1. However, since this would require realignment of the target polarization for each value of $\boldsymbol{q}$, experiments are performed with the deuteron polarization generally fixed along the direction of the electron beam defined by $\boldsymbol{k}$. This involves a right-handed rotation of the deuteron density matrix about the y axis through the angle between $\boldsymbol{q}$ and $\boldsymbol{k}$ denoted by θ_{kq} resulting in a new set of polarization coefficients $\widetilde{T}_{JM}$. This rotation is described in detail in Appendix B. Equation (B8) relates T_{JM} to $\widetilde{T}_{JM}$.

B. Asymmetries

Conventionally, target polarization in deuteron electrodisintegration is measured in terms of four single asymmetries

$$A_d^V = \frac{v_L R_L(\widetilde{T}_{10}) + v_T R_T(\widetilde{T}_{10}) + v_{TT} R_{TT}(\widetilde{T}_{10}) + v_{LT} R_{LT}(\widetilde{T}_{10})}{\widetilde{T}_{10}\Sigma},$$

$$A_d^T = \frac{v_L R_L(\widetilde{T}_{20}) + v_T R_T(\widetilde{T}_{20}) + v_{TT} R_{TT}(\widetilde{T}_{20}) + v_{LT} R_{LT}(\widetilde{T}_{20})}{\widetilde{T}_{20}\Sigma},$$

$$A_{ed}^V = \frac{v_{LT'} R_{LT'}(\widetilde{T}_{10}) + v_{T'} R_{T'}(\widetilde{T}_{10})}{\widetilde{T}_{10}\Sigma},$$

$$A_{ed}^T = \frac{v_{LT'} R_{LT'}(\widetilde{T}_{20}) + v_{T'} R_{T'}(\widetilde{T}_{20})}{\widetilde{T}_{20}\Sigma}, \tag{7}$$

where

$$\Sigma = v_L R_L(U) + v_T R_T(U) + v_{TT} R_{TT}(U) + v_{LT} R_{LT}(U). \tag{8}$$

Here, $R_i(\widetilde{T}_{10})$ and $R_i(\widetilde{T}_{20})$ denote the response functions where only $\widetilde{T}_{10}$ is nonzero or only $\widetilde{T}_{20}$ is nonzero. $R_i(U)$ denotes the unpolarized response functions. In Eq. (7) the superscripts V and T refer to vector and tensor polarizations. The subscript d indicates that all of these asymmetries are defined for polarized deuterons. The subscript e denotes the case where the electron beam is also polarized.

C. Factorization

The Feynman diagrams representing current matrix element deuteron electrodisintegration for the Bethe-Salpeter equation are shown in Fig. 2. Figures 2(a) and 2(b) have plane wave (PW) final states while Figs. 2(c) and 2(d) include final state interactions (FSI). Figures 2(e) and 2(f) contain two-body currents with plane wave final state and FSI, respectively.

Any attempt to evaluate the effects of d-state contributions to the deuteron wave function require that the cross section can be factored into an effective single-nucleon cross section and a

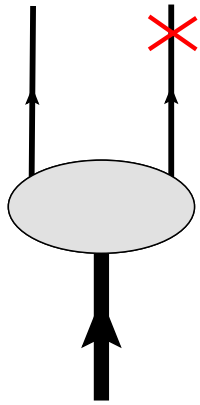

FIG. 3. Feynman diagram representing the half-off-shell vertex function.

momentum distribution. This can only occur if Figs. 2(b)–2(f) make negligible contributions to the current matrix element.

The plane wave contribution to the current matrix element represented by Fig. 2(a) can then be written as

$$\langle \boldsymbol{p}_1 s_1; \boldsymbol{p}_2 s_2 | J^{\mu}_{(1)} | \boldsymbol{P} \lambda_d \rangle_a = -\bar{u}(\boldsymbol{p}_1, s_1)\Gamma^{\mu}(q) G_0(P - p_2) \times \Gamma^{T}_{\lambda_d}(p_2, P)\bar{u}^{T}(\boldsymbol{p}_2, s_2), \quad (9)$$

where the nucleon propagator is

$$G_0(p) = \frac{\gamma \cdot p + m_N}{m_N^2 - p^2} \quad (10)$$

and the one-body nucleon electromagnetic current operator is chosen to be of the Dirac-plus-Pauli form

$$\Gamma^{\mu}(q) = F_1(Q^2)\gamma^{\mu} + \frac{F_2(Q^2)}{2m_N} i\sigma^{\mu\nu} q_{\nu}. \quad (11)$$

The deuteron vertex function with particle 2 on shell, as required by Fig. 2(a) is shown in Fig. 3 and is given in general by

$$\Gamma_{\lambda_d}(p_2, P) = \Big[g_1\big(p_2^2, p_2 \cdot P\big)\gamma \cdot \xi_{\lambda_d}(P) - g_2\big(p_2^2, p_2 \cdot P\big)\frac{p_2 \cdot \xi_{\lambda_d}(P)}{m_N} - \Big(g_3\big(p_2^2, p_2 \cdot P\big)\gamma \cdot \xi_{\lambda_d}(P) - g_4\big(p_2^2, p_2 \cdot P\big)\frac{p_2 \cdot \xi_{\lambda_d}(P)}{m_N} \Big)\frac{\gamma \cdot (P - p_2) + m}{m_N} \Big] C, \quad (12)$$

where $\xi_{\lambda_d}(P)$ is the deuteron polarization four-vector, C is the charge conjugation matrix, and the invariant functions $g_i(p_2^2, p_2 \cdot P)$ are given by

$$g_1\big(p_2^2, p_2 \cdot P\big) = \frac{(2E_{p_R} - M_d)(p_R \Psi_3(p_R) - m_N \Psi_4(p_R))}{4\sqrt{\pi}\, p_R}, \quad (13)$$

$$g_2\big(p_2^2, p_2 \cdot P\big) = \frac{m_N(2E_{p_R} - M_d)(\sqrt{2}E_{p_R}\Psi_1(p_R) - m_N\Psi_3(p_R) - p_R\Psi_4(p_R))}{4\sqrt{\pi}\, p_R^2}, \quad (14)$$

$$g_3\big(p_2^2, p_2 \cdot P\big) = -\frac{E_{p_R} m_N \Psi_4(p_R)}{4\sqrt{\pi}\, p_R}, \quad (15)$$

$$g_4\big(p_2^2, p_2 \cdot P\big) = \frac{m_N^2}{4\sqrt{\pi} M_d p_R^2}\big(-2E_{p_R}^2\Psi_3(p_R) + E_{p_R}\big(M_d\Psi_3(p_R) + 2\sqrt{2}m_N\Psi_1(p_R)\big) + \sqrt{2}M_d(p_R\Psi_2(p_R) - m_N\Psi_1(p_R))\big), \quad (16)$$

where

$$p_R = \sqrt{\frac{(P \cdot p_2)^2}{P^2} - p_2^2} \quad (17)$$

is the relative momentum of the nucleons in the rest frame of the deuteron and

$$\Psi_1(p_R) = u(p_R) + \sqrt{2}w(p_R), \quad (18)$$

$$\Psi_2(p_R) = -\sqrt{3}v_s(p_R), \quad (19)$$

$$\Psi_3(p_R) = \sqrt{2}u(p_R) - w(p_R), \quad (20)$$

$$\Psi_4(p_R) = -\sqrt{3}v_t(p_R). \quad (21)$$

Here, $u(p)$ is the s-wave radial wave function, $w(p)$ is the d-wave radial wave function, and $v_s(p)$ and $v_t(p)$ are singlet and triplet p-wave radial wave functions.

It is convenient to define a half-off-shell wave function as

$$\psi_{\lambda_d, s_2}(p_2, P) = G_0(P - p_2)\Gamma^{T}_{\lambda_d}(p_2, P)\bar{u}^{T}(\boldsymbol{p}_2, s_2). \quad (22)$$

We choose to normalize this wave function such that in the deuteron in any frame

$$\sum_{s_2}\int \frac{d^3 p_2}{(2\pi)^3}\frac{m}{E_{p_2}}\bar{\psi}_{\lambda_d, s_2}(p_2, P)\gamma^{\mu}\psi_{\lambda_d, s_2}(p_2, P) = \frac{P^{\mu}}{M_d}, \quad (23)$$

which is correct only in the absence of energy-dependent kernels. This results in the normalization of the radial wave functions in the deuteron rest frame being

$$1 = \int_0^{\infty}\frac{dpp^2}{(2\pi)^3}\big[u^2(p) + w^2(p) + v_t^2(p) + v_s^2(p)\big] = \frac{1}{3}\int_0^{\infty}\frac{dpp^2}{(2\pi)^3}\big[\Psi_1^2(p) + \Psi_2^2(p) + \Psi_3^2(p) + \Psi_4^2(p)\big] \quad (24)$$

In the deuteron rest frame we choose the four-momenta such that

$$p_1 = p_p = \left(E_{p_1}, \boldsymbol{p}_1\right), \tag{25}$$

$$p_2 = (E_p, -\boldsymbol{p}), \tag{26}$$

$$P = (M_d, \boldsymbol{0}), \tag{27}$$

$$q = (\nu, \boldsymbol{q}). \tag{28}$$

The four-momentum of the struck nucleon is given by

$$l = P - p_2 = (M_d - E_p, \boldsymbol{p}) = (E_p, \boldsymbol{p}) + (M_d - 2E_p, \boldsymbol{0}) = p + \Delta, \tag{29}$$

where

$$p = (E_p, \boldsymbol{p}) \tag{30}$$

is on shell and

$$p_R = |\boldsymbol{p}|. \tag{31}$$

The of-fshell contribution to the momentum of the struck nucleon is

$$\Delta = (M_d - 2E_p, \boldsymbol{0}) = (\delta, \boldsymbol{0}). \tag{32}$$

The PWIA response tensor is then

$$\begin{aligned} W_{aa}^{\mu\nu} &= \sum_{s_1, s_2, \lambda_d, \lambda_{d'}} \overline{\psi}_{\lambda_{d'}, s_2}(p_2, P)\Gamma^{\mu}(-q)u(\boldsymbol{p}_1, s_1)\bar{u}(\boldsymbol{p}_1, s_1) \\ &\quad \times \Gamma^{\nu}(q)\psi_{\lambda_d, s_2}(p_2, P)\rho_{\lambda_d, \lambda_{d'}} \\ &= \mathrm{Tr}[\Gamma^{\mu}(-q)\Lambda_+(\boldsymbol{p}_1)\Gamma^{\nu}(q)N(p_2, P)], \end{aligned} \tag{33}$$

where the momentum distribution operator is given by

$$N(p_2, P) = \sum_{s_2, \lambda_d, \lambda_{d'}} \psi_{\lambda_d, s_2}(p_2, P)\rho_{\lambda_d, \lambda_{d'}}\overline{\psi}_{\lambda_{d'}, s_2}(p_2, P). \tag{34}$$

The deuteron density matrix can be written as

$$\boldsymbol{\rho}^D = \frac{1}{3}\left[\sum_{J=0}^{2} T_{J0}\boldsymbol{\tau}_{J0} + \sum_{J=1}^{2}\sum_{M=1}^{J}\left(\Re(T_{JM})\boldsymbol{\tau}_{JM}^{\Re} + \Im(T_{JM})\boldsymbol{\tau}_{JM}^{\Im}\right)\right]. \tag{35}$$

where $T_{00} = 1$ and the matrices $\boldsymbol{\tau}_{JM}$ are defined as

$$\boldsymbol{\tau}_{00} = \begin{pmatrix} 1 & 0 & 0 \\ 0 & 1 & 0 \\ 0 & 0 & 1 \end{pmatrix}, \quad \boldsymbol{\tau}_{10} = \sqrt{\frac{3}{2}}\begin{pmatrix} 1 & 0 & 0 \\ 0 & 0 & 0 \\ 0 & 0 & -1 \end{pmatrix},$$

$$\boldsymbol{\tau}_{20} = \frac{1}{\sqrt{2}}\begin{pmatrix} 1 & 0 & 0 \\ 0 & -2 & 0 \\ 0 & 0 & 1 \end{pmatrix},$$

$$\boldsymbol{\tau}_{11}^{\Re} = \sqrt{\frac{3}{2}}\begin{pmatrix} 0 & -1 & 0 \\ -1 & 0 & -1 \\ 0 & -1 & 0 \end{pmatrix}, \quad \boldsymbol{\tau}_{11}^{\Im} = \sqrt{\frac{3}{2}}\begin{pmatrix} 0 & i & 0 \\ -i & 0 & i \\ 0 & -i & 0 \end{pmatrix},$$

$$\boldsymbol{\tau}_{21}^{\Re} = \sqrt{\frac{3}{2}}\begin{pmatrix} 0 & -1 & 0 \\ -1 & 0 & 1 \\ 0 & 1 & 0 \end{pmatrix}, \quad \boldsymbol{\tau}_{21}^{\Im} = \sqrt{\frac{3}{2}}\begin{pmatrix} 0 & i & 0 \\ -i & 0 & -i \\ 0 & i & 0 \end{pmatrix},$$

$$\boldsymbol{\tau}_{22}^{\Re} = \sqrt{3}\begin{pmatrix} 0 & 0 & 1 \\ 0 & 0 & 0 \\ 1 & 0 & 0 \end{pmatrix}, \quad \boldsymbol{\tau}_{22}^{\Re} = \sqrt{3}\begin{pmatrix} 0 & 0 & -i \\ 0 & 0 & 0 \\ i & 0 & 0 \end{pmatrix}. \tag{36}$$

Note that these matrices are all hermitian. The polarization coefficients can be extracted from the density matrix using

$$T_{J0} = \mathrm{Tr}\left[\boldsymbol{\tau}_{JM}^{\Re}\boldsymbol{\rho}^D\right], \tag{37}$$

$$\Re(T_{JM}) = \tfrac{1}{2}\mathrm{Tr}\left[\boldsymbol{\tau}_{JM}^{\Re}\boldsymbol{\rho}^D\right], \tag{38}$$

$$\Im(T_{JM}) = \tfrac{1}{2}\mathrm{Tr}\left[\boldsymbol{\tau}_{JM}^{\Im}\boldsymbol{\rho}^D\right]. \tag{39}$$

Using Eqs. (35), (36), and (39), the momentum distribution operator can be written as

$$\begin{aligned} N(p_2, P) = &\sum_{J=0}^{2} N_{J0}(p_2, P)T_{J0} \\ &+ \sum_{J=1}^{2}\sum_{M=1}^{J}[\Re(N_{JM}(p_2, P))\Re(T_{JM}) \\ &+ \Im(N_{JM}(p_2, P))\Im(T_{JM})]. \end{aligned} \tag{40}$$

This is an operator in the four-dimensional Dirac spinor space and can be expanded in terms of γ matrices such that, for $J = 0$ or $J = 2$,

$$\begin{aligned} N_{JM}(p_2, P) = \frac{1}{8\pi}\big[&\mathcal{N}_{tv}(p_2, P)n_{tv}^{JM}(\boldsymbol{p}) + \mathcal{N}_{sv}(P, p2)n_{sv}^{JM}(\boldsymbol{p}) \\ &+ \mathcal{N}_s(p_2, P)n_s^{JM}(\boldsymbol{p})\big], \end{aligned} \tag{41}$$

where

$$\mathcal{N}_{tv}(p_2, P) = \frac{1}{2}\frac{P \cdot p_2}{M_d^2 m_N}\gamma \cdot P, \tag{42}$$

$$\mathcal{N}_{sv}(p_2, P) = \frac{1}{2}\left(\frac{P \cdot p_2}{M_d^2 m_N}\gamma \cdot P - \frac{\gamma \cdot p_2}{m_n}\right), \tag{43}$$

$$\mathcal{N}_s(p_2, P) = \frac{1}{2}, \tag{44}$$

and, for $J = 1$,

$$\begin{aligned} N_{1M}(p_2, P, s) = \frac{1}{8\pi}\big[&\mathcal{N}_{tav}(p_2, P, s)n_{tav}^{1M}(\boldsymbol{p}) \\ &+ \mathcal{N}_{sav}(p_2, P, s)n_{sav}^{1M}(\boldsymbol{p}) \\ &+ \mathcal{N}_{at}(P, p_2, s)n_{at}^{1M}(\boldsymbol{p})\big], \end{aligned} \tag{45}$$

where

$$\mathcal{N}_{tav}(p_2, P, s) = \frac{1}{2}\frac{P \cdot s}{M_d^2}\gamma \cdot P\gamma_5, \tag{46}$$

$$\mathcal{N}_{sav}(p_2, P, s) = \frac{1}{2}\left(\gamma \cdot s - \frac{P \cdot s}{M_d^2}\gamma \cdot P\right)\gamma_5, \tag{47}$$

$$\mathcal{N}_{at}(p_2, P, s) = -\frac{i}{2}\frac{m_N}{P \cdot p_2}\sigma^{\alpha\beta}P_{\alpha}s_{\beta}\gamma_5, \tag{48}$$

and

$$s = \left(\frac{|\boldsymbol{p}|}{m_N}, \frac{E_p}{m_N}\hat{p}\right) \tag{49}$$

is the spin-four-vector for rest-frame spin aligned along $\hat{p}$.

The nine momentum distributions are given by

$$n_{tv}^{00}(p) = \frac{1}{3}\big(\Psi_1^2(p) + \Psi_2^2(p) + \Psi_3^2(p) + \Psi_4^2(p)\big), \tag{50}$$

$$n_{sv}^{00}(p) = \frac{1}{3}\bigg(\big(\Psi_1^2(p) - \Psi_2^2(p) + \Psi_3^2(p) - \Psi_4^2(p)\big) + 2\frac{m_N}{p}(\Psi_1(p)\Psi_2(p) - \Psi_3(p)\Psi_4(p))\bigg), \tag{51}$$

$$n_{s}^{00}(p) = \frac{1}{3}\bigg(\big(\Psi_1^2(p) - \Psi_2^2(p) + \Psi_3^2(p) - \Psi_4^2(p)\big) + \frac{p}{m_N}(2\Psi_3(p)\Psi_4(p) - 2\Psi_1(p)\Psi_2(p))\bigg),$$

$$n_{tav}^{1M}(\boldsymbol{p}) = -\frac{\eta_M}{3}\sqrt{2\pi}\bigg(\big(\Psi_3^2(p) - \Psi_4^2(p)\big) - 2\frac{m_N}{p}\Psi_3(p)\Psi_4(p)\bigg)Y_{1M}(\Omega_p), \tag{52}$$

$$n_{sav}^{1M}(\boldsymbol{p}) = -\frac{\eta_M}{3}\sqrt{2\pi}\big(\Psi_3^2(p) + \Psi_4^2(p)\big)Y_{1M}(\Omega_p), \tag{53}$$

$$n_{at}^{1M}(\boldsymbol{p}) = -\frac{\eta_M}{3}\sqrt{2\pi}\bigg(\big(\Psi_3^2(p) - \Psi_4^2(p)\big) + 2\frac{p}{m_N}\Psi_3(p)\Psi_4(p)\bigg)Y_{1M}(\Omega_p),$$

$$n_{tv}^{2M}(\boldsymbol{p}) = -\frac{\eta_M}{3}\sqrt{\frac{2\pi}{5}}\big(2\Psi_1^2(p) + 2\Psi_2^2(p) - \Psi_3^2(p) - \Psi_4^2(p)\big)Y_{2M}(\Omega_p), \tag{54}$$

$$n_{sv}^{2M}(\boldsymbol{p}) = -\frac{\eta_M}{3}\sqrt{\frac{2\pi}{5}}\bigg(\big(2\Psi_1^2(p) - 2\Psi_2^2(p) - \Psi_3^2(p) + \Psi_4^2(p)\big) + 2\frac{m_N}{p}(2\Psi_1(p)\Psi_2(p) + \Psi_3(p)\Psi_4(p))\bigg)Y_{2M}(\Omega_p), \tag{55}$$

$$n_{s}^{2M}(\boldsymbol{p}) = -\frac{\eta_M}{3}\sqrt{\frac{2\pi}{5}}\bigg(\big(2\Psi_1^2(p) - 2\Psi_2^2(p) - \Psi_3^2(p) + \Psi_4^2(p)\big) - 2\frac{p}{m_N}(2\Psi_1(p)\Psi_2(p) + \Psi_3(p)\Psi_4(p))\bigg)Y_{2M}(\Omega_p), \tag{56}$$

where

$$\eta_M = \begin{cases} 1 & \text{for} \quad M = 0 \\ 2 & \text{for} \quad M > 0 \end{cases}. \tag{57}$$

If the p waves are neglected then $\Psi_2 \to 0$ and $\Psi_4 \to 0$. The momentum distributions then simplify to

$$n_+^{00} = n_{tv}^{00}(p) = n_{sv}^{00}(p) = n_s^{00}(p) = \frac{1}{3}\big(\Psi_1^2(p) + \Psi_3^2(p)\big), \tag{58}$$

$$n_+^{1M}(\boldsymbol{p}) = n_{tav}^{1M}(\boldsymbol{p}) = n_{sav}^{1M}(\boldsymbol{p}) = n_{at}^{1M}(\boldsymbol{p}) = -\frac{\eta_M}{3}\sqrt{2\pi}\Psi_3^2(p)Y_{1M}(\Omega_p), \tag{59}$$

$$n_+^{2M}(\boldsymbol{p}) = n_{tv}^{2M}(\boldsymbol{p}) = n_{sv}^{2M}(\boldsymbol{p}) = n_s^{2M}(\boldsymbol{p}) = -\frac{\eta_M}{3}\sqrt{\frac{2\pi}{5}}\big(2\Psi_1^2(p) - \Psi_3^2(p)\big)Y_{2M}(\Omega_p). \tag{60}$$

These can be rewritten in terms of u and w using

$$\tfrac{1}{3}\big(\Psi_1^2(p) + \Psi_3^2(p)\big) = u^2(p) + w^2(p), \tag{61}$$

$$\tfrac{1}{3}\Psi_3^2(p) = \tfrac{1}{3}(2u(p)^2 - 2\sqrt{2}u(p)w(p) + w(p)^2), \tag{62}$$

$$\tfrac{1}{3}\big(2\Psi_1^2(p) - \Psi_3^2(p)\big) = w(p)(2\sqrt{2}u(p) + w(p)). \tag{63}$$

These are in agreement with the usual nonrelativistic polarized momentum distributions up to a factor determined by our choice for the normalization of the wave functions [50,51].

Since all of the momentum distributions are now the same for each J and M, these can now be factored out and leave the combinations of operators

$$\mathcal{N}_{tv}(p_2,P) + \mathcal{N}_{sv}(p_2,P) + \mathcal{N}_{s}(p_2,P) = \Lambda_+(\boldsymbol{p}) \tag{64}$$

for $J = 0,2$ and

$$\mathcal{N}_{tav}(p_2,P) + \mathcal{N}_{sav}(p_2,P) + \mathcal{N}_{at}(p_2,P) = \frac{1}{2}\bigg[\gamma\cdot s - \frac{i}{2}\frac{m_N}{P\cdot p_2}\sigma^{\alpha\beta}P_\alpha s_\beta\bigg]\gamma_5 \tag{65}$$

for $J = 1$:

$$N(p_2,P) = \frac{1}{8\pi}\bigg\{\Lambda_+(\boldsymbol{p})\bigg[n_+^{00}(p) + n_+^{20}(\boldsymbol{p})T_{20} + \sum_{M=1}^{2}[\Re(n_+^{2M}(\boldsymbol{p}))\Re(T_{2M}) + \Im(n_+^{2M}(\boldsymbol{p}))\Im(T_{2M})]\bigg] + \frac{1}{2}\bigg[\gamma\cdot s - \frac{i}{2}\frac{m_N}{P\cdot p_2}\sigma^{\alpha\beta}P_\alpha s_\beta\bigg]\gamma_5 \times [n_+^{10}(\boldsymbol{p})T_{20} + \Re(n_+^{11}(\boldsymbol{p}))\Re(T_{11}) + \Im(n_+^{11}(\boldsymbol{p}))\Im(T_{11}))]\bigg\}. \tag{66}$$

The factored cross section can then be written as

$$\frac{d\sigma^5}{d\epsilon' d\Omega_e d\Omega_p} = \frac{m_p\, m_n\, p_1}{8\pi^3\, M_d}\,\sigma_{\text{Mott}}\, f_{\text{rec}}^{-1}\bigg\{\big[v_L r_L^{(I)} + v_T r_T^{(I)} + v_{TT} r_{TT}^{(I)}\cos 2\phi + v_{LT} r_{LT}^{(I)}\cos\phi\big] \times \bigg[n_+^{00}(\boldsymbol{p}_m) + n_+^{20}(\boldsymbol{p}_m)T_{20} + \sum_{M=1}^{2}[\Re(n_+^{2M}(\boldsymbol{p}_m))\Re(T_{2M}) + \Im(n_+^{2M}(\boldsymbol{p}_m))\Im(T_{2M})]\bigg] + h\big[v_{LT'} r_{LT'}^{(II)}\cos\phi + v_{T'} r_{T'}^{(II)}\big] \times \big[n_+^{10}(\boldsymbol{p}_m)T_{10} + \Re(n_+^{11}(\boldsymbol{p}_m))\Re(T_{11}) + \Im(n_+^{11}(\boldsymbol{p}_m))\Im(T_{11})\big]\bigg\}, \tag{67}$$

where the effective reduced single-nucleon response functions are listed in Appendix C and are related to the conventional deForest CC2 prescription [5] up to normalization factors. Note that contributions from vector polarization of the deuteron contribute to the factored cross section only when the electron beam is also polarized. The single-nucleon contributions for unpolarized electrons are the same for both unpolarized and tensor polarized deuterons.

Assuming that $\widetilde{T}_{JM} \neq 0$ only for $J = 2$ and $M = 0$ and using Eq. (B8) the tensor asymmetry for the factored cross section can be written as

$$\begin{aligned}(A_d^T)_{\text{factored}} &= \frac{n_+^{20}(\boldsymbol{p}_m)T_{20} + \Re(n_+^{21}(\boldsymbol{p}_m))\Re(T_{21}) + \Re(n_+^{22}(\boldsymbol{p}_m))\Re(T_{22})}{n_+^{00}(\boldsymbol{p}_m)\widetilde{T}_{20}} \\ &= \frac{n_+^{20}(\boldsymbol{p}_m)\frac{1}{4}(1+3\cos 2\theta_{kq}) + \Re(n_+^{21}(\boldsymbol{p}_m))\sqrt{\frac{3}{8}}\sin 2\theta_{kq} + \Re(n_+^{22}(\boldsymbol{p}_m))\sqrt{\frac{3}{32}}(1-\cos 2\theta_{kq})}{n_+^{00}(\boldsymbol{p}_m)} \\ &= -\sqrt{\frac{2\pi}{5}}\frac{2\Psi_1^2(p_m) - \Psi_3^2(p_m)}{\Psi_1^2(p_m) + \Psi_3^2(p_m)}\Xi(\theta_m,\phi,\theta_{kq}),\end{aligned} \tag{68}$$

where the factored effective single-proton cross section is canceled since it is the same for both the numerator and denominator. The angular factor is defined as

$$\begin{aligned}\Xi(\theta_m,\phi,\theta_{kq}) &= \left[\frac{1}{4}(1+3\cos 2\theta_{kq})Y_{20}(\Omega_p) + \sqrt{\frac{3}{2}}\sin 2\theta_{kq}\Re(Y_{21}(\Omega_p)) + \sqrt{\frac{3}{8}}(1-\cos 2\theta_{kq})\Re(Y_{22}(\Omega_p))\right] \\ &= \sqrt{\frac{5}{64\pi}}\left[\frac{1}{4}(1+3\cos 2\theta_{kq})(1+3\cos 2\theta_m) - 3\sin 2\theta_{kq}\sin 2\theta_m\cos\phi + \frac{3}{4}(1-\cos\theta_{kq})(1-\cos\theta_m)\cos 2\phi\right].\end{aligned} \tag{69}$$

If we define a reduced tensor asymmetry as

$$a_d^T = \frac{A_d^T}{\Xi(\theta_m,\phi,\theta_{kq})}. \tag{70}$$

Then the factored reduced tensor asymmetry is

$$\left(a_d^T\right)_{\text{factored}} = -\sqrt{\frac{2\pi}{5}}\frac{w(p_m)(2\sqrt{2}u(p_m) + w(p_m))}{u^2(p_m) + w^2(p_m)} \tag{71}$$

independent of all kinematical variables except the missing momentum p_m. If Eq. (71) correctly represents the reduced asymmetry a_d^T then this expression can be solved to obtain the ratio of s to d state wave functions. This solution requires that

$$-2\sqrt{\frac{2\pi}{5}} \leqslant a_d^T \leqslant \sqrt{\frac{2\pi}{5}}. \tag{72}$$

If p_- is defined such that

$$a_d^T(p_-) = -2\sqrt{\frac{2\pi}{5}} \tag{73}$$

and p_+ is defined such that

$$a_d^T(p_+) = \sqrt{\frac{2\pi}{5}}, \tag{74}$$

then

$$\frac{u(p_m)}{w(p_m)} = \begin{cases} \frac{-\sqrt{5}\sqrt{-5a_d^{T\,2} - \sqrt{10\pi}a_d^T + 4\pi} - 2\sqrt{5\pi}}{5a_d^T} & \text{for} \quad 0 \leqslant p_m < p_- \text{ or } p_m > p_+ \\ \frac{\sqrt{5}\sqrt{-5a_d^{T\,2} - \sqrt{10\pi}a_d^T + 4\pi} - 2\sqrt{5\pi}}{5a_d^T} & \text{for} \quad p_- \leqslant p_m \leqslant p_+ \end{cases}. \tag{75}$$

In Sec. III, we investigate numerically the behavior of the reduced asymmetry when it is calculated using final state interactions, and various versions of commonly use d-wave functions and form factor parametrizations. We will observe there that factorization breaks down, and that the use of Eq. (71) is unrealistic.

III. RESULTS

Independent of the dynamical model for the description of the $\vec{H}^2(e,e'p)$ reaction, every calculation needs a wave function, nucleon form factor parametrizations, and nucleon-nucleon amplitudes as inputs. We list the model inputs used in

TABLE I. Model inputs to the calculation.

Final state interactions	Form factors	Deuteron wave function
		IIB [63]
		WJC 1 [64]
Regge	GKex05 [59,60]	WJC 2 [64]
[53–55]		AV18 [65]
SAID	AMT [61]	CD Bonn [66]
[56–58]	MMD [62]	NIMJ 1 [67]
		NIMJ 2 [67]
		NIMJ 3 [67]

our calculations in Table I. The reasons for these choices are discussed in more detail in [52].

We start out by showing the influence of the different wave functions on the factored, reduced asymmetry a_d^T, as defined by Eq. (71), in Fig. 4. Note that the factored, reduced asymmetry does not depend on the nucleon form factors, so the only model input necessary is the wave function. For missing momenta larger than 0.3 GeV, the curves start to deviate from each other, and they fan out considerably for $p_m \approx 0.6$ GeV and larger. Most wave functions lead to similar asymmetries, with the exception of the CD Bonn that has a slightly different shape, peaking at high p_m, and the Nijmegen 3 wave function that leads to the lowest values for the factored, reduced a_d^T at the high p_m. This indicates that constraining the interactions to fit NN scattering up to just above the π-production threshold and to give the correct deuteron binding energy is insufficient to uniquely determine the wave function above $p_m \simeq 0.3$ GeV. The corresponding s to d ratios are shown in Fig. 5.

When comparing the results shown in Fig. 4 to the numbers for the d wave content of the various wave functions in Table II, it is obvious that there is no direct relationship between the d-wave content and the size of the reduced asymmetry calculated with a particular wave function. Depending on the missing momentum, e.g., the CD Bonn wave function result is either below the others (for $p_m < 0.6$ GeV), or above the

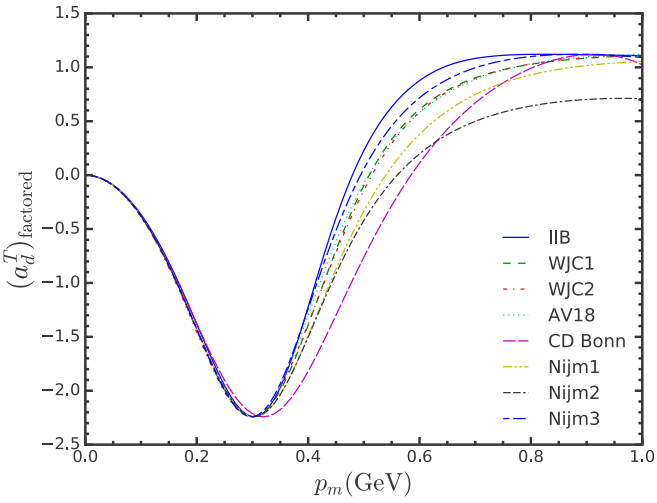

FIG. 4. The factored, reduced asymmetry a_d^T calculated for the eight different wave functions used in our calculations.

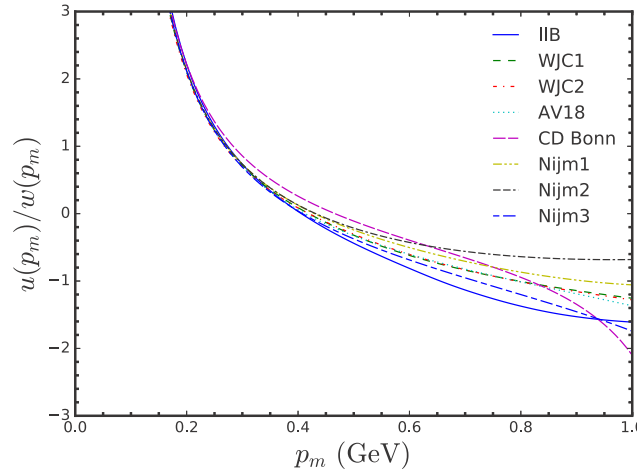

FIG. 5. The ratio $u(p)/w(p)$ calculated for the eight different wave functions used in our calculations.

others around $p_m \approx 0.9$ GeV. CD Bonn has the lowest d state probability of all considered wave functions. Nijmegen 2 and Nijmegen 3 have almost identical d wave contents—5.68% versus 5.65%—but are rather different, with Nijmegen 2 leading to a much smaller asymmetry than Nijmegen 3 for $p_m > 0.5$ GeV.

A more realistic calculation includes the Born approximation graph, where the photon couples to the neutron, and final state interactions. At this point, the parametrizations of the nucleon form factors and of the nucleon-nucleon amplitudes enter. As eight wave functions, three form factor parametrizations, and two nucleon-nucleon amplitude parametrizations lead to $8 \times 3 = 24$ possible combinations for PWBA and to $8 \times 3 \times 2 = 48$ possible combinations for the DWBA (henceforth referred to as FSI) and therefore lead to very busy plots, we only show the envelope of the PWBA and FSI calculations in the figures.

We remark in passing that the differences between PWIA and PWBA calculations for the same choice of model inputs is tiny. The difference is apparent in the numbers, but does not show up on a plot of the scale we use for the figures in this paper. The use of different form factor parametrizations in PWBA leads to a relatively larger, but absolutely still very small difference that is not visible at the scale used.

The difference between the PWBA and the factored version of the PWBA, which excludes p waves, is small but visible

TABLE II. Wave function probabilities.

	s wave	d wave	Triplet p wave	Singlet p wave
IIB	94.82%	5.11%	0.06%	0.01%
WJC 1	92.33%	7.34%	0.11%	0.21%
WJC 2	93.60%	6.38%	0.01%	0.01%
AV18	94.24%	5.76%	0.00%	0.00%
CD Bonn	95.15%	4.85%	0.00%	0.00%
NIJM 1	94.25%	5.75%	0.00%	0.00%
NIJM 2	94.32%	5.68%	0.00%	0.00%
NIJM 3	94.35%	5.65%	0.00%	0.00%

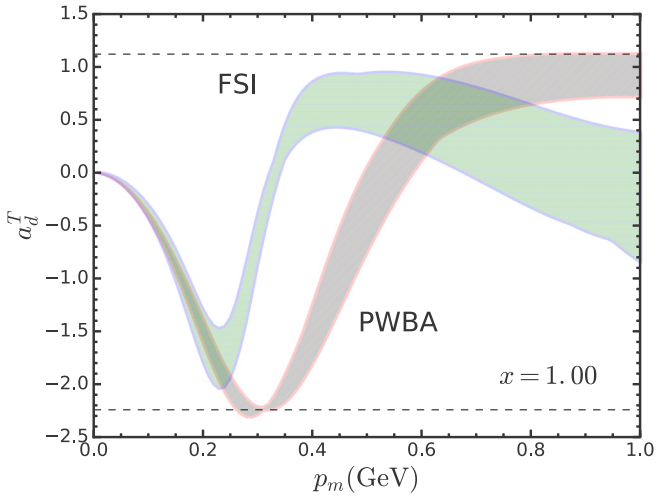

FIG. 6. The envelopes of the reduced asymmetry a_d^T calculated in PWBA and with FSI, for $x = 1.00$, $Q^2 = 2.4$ GeV^2, $\varepsilon = 8.3$ GeV, and $\phi = 165^\circ$. The horizontal dashed lines indicate the limits required by Eqs. (73) and (74).

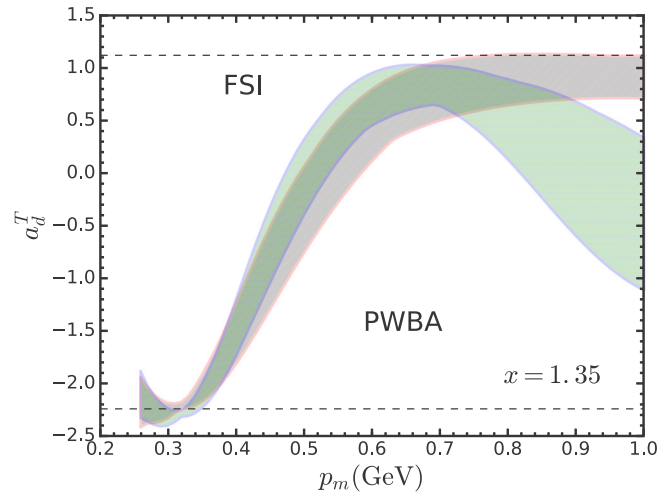

FIG. 7. The envelopes of the reduced asymmetry a_d^T calculated in PWBA and with FSI, for $x = 1.35$, $Q^2 = 4.25$ GeV^2, $\varepsilon = 11$ GeV, and $\phi = 165^\circ$. The horizontal dashed lines indicate the limits required by Eqs. (73) and (74).

at medium and high missing momentum when plotted for relativistic wave functions. The non-relativistic wave functions still show a difference between factored and unfactored PWBA, but this is tiny as it is practically the difference between PWIA and PWBA.

In Fig. 6 we show the envelopes for the PWBA and FSI calculations for $x = 1.00$. The differences in the PWBA calculations mainly stem from the different wave functions used, and the PWBA envelope shown mainly corresponds to the PWIA curves of Fig. 4. Once FSIs are included, the asymmetry changes shape, and the dip moves to lower values of the missing momentum, as observed already in [34]. For FSI, the different model inputs now lead to a significant spread for missing momenta above 0.35 GeV, as well as in the dip of the asymmetry at lower p_m. For high missing momentum, the uncertainties introduced by the model inputs in FSI are more than twice as large as for PWBA.

We now consider kinematics at $x = 1.35$, away from the quasielastic peak. Our results are shown in Fig. 7. As for $x = 1.00$, the FSI calculation envelope shows a much larger spread due to the model inputs than the PWBA envelope, in particular for missing momenta larger than 0.7 GeV. While in the factored version of the calculation, i.e., in PWIA without p waves, the results are completely independent of x, it is obvious from comparing Figs. 6 and 7 that FSIs introduce a quite drastic dependence on kinematic variables beyond the missing momentum.

IV. SUMMARY AND OUTLOOK

In this paper, first we considered the tensor asymmetry A_d^T within a relativistic framework. We investigated the conditions under which this asymmetry can be factored. We defined a reduced asymmetry a_d^T that factors in PWIA when the p waves are neglected. The factored version of the reduced asymmetry depends on the missing momentum only. It agrees with the well-known nonrelativistic version.

Then, we presented numerical results for the reduced tensor asymmetry a_d^T and compared these results to the factored version $(a_T^d)_{\text{factored}}$. While we have shown analytically and numerically that factorization holds in PWIA in the absence of p waves, the numerical results imply that factorization is broken thoroughly once FSIs are included. The inclusion of FSIs leads to changes in shape of the reduced asymmetry, in particular at high missing momentum. The FSIs also introduce a significant dependence on x (and other kinematics variables) besides the missing momentum, thus making the breaking of factorization obvious. This is consistent with [34,35]. The only region where the factorization holds approximately is at very low missing momenta of 200 MeV or less.

We also have demonstrated numerically that there is no systematic relationship of the form of $(a_d^T)_{\text{factored}}$ to the d-wave probability of the various wave functions.

We would like to point out that the tensor asymmetry is a special case: the vector asymmetry A_d^V as defined in [34] does not factorize at all, not even in PWIA without p-waves. Therefore, we feel that the tensor asymmetry A_d^T is the best observable for the exploration of the d wave, unless one wishes to consider experiments with polarized target and polarized beam. These double-polarization are much harder to perform, though.

Our results imply that extracting any information on the d-wave content of the wave function—which is, after all, not an observable—from the tensor asymmetry A_d^T will require an extremely careful treatment of the reaction dynamics, and will carry a theoretical uncertainty due to the many, equally valid model inputs necessary. It is important to keep in mind that, completely apart from which contributions to the reaction mechanism are evaluated in a theory calculation, and in which way, the model inputs will always generate a considerable uncertainty. Theoretical results should therefore always be

given as an envelope to fairly represent the uncertainties, not as single curves. The kinematics at large x and medium values of p_m might be best suited to any attempt to learn about the d-wave content.

ACKNOWLEDGMENTS

This work was supported in part by funds provided by the US Department of Energy (DOE) under cooperative research Agreement No. DE-AC05-84ER40150 and by the National Science Foundation under Grant No. PHY-1306250. Notice: Authored by Jefferson Science Associates, LLC under U.S. DOE Contract No. DE-AC05-06OR23177. The U.S. Government retains a non-exclusive, paid-up, irrevocable, world-wide license to publish or reproduce this manuscript for U.S. Government purposes.

APPENDIX A: KINEMATIC FACTORS AND RESPONSE FUNCTIONS

The leptonic coefficients v_K are

$$v_L = \frac{Q^4}{q^4}, \tag{A1}$$

$$v_T = \frac{Q^2}{2q^2} + \tan^2\frac{\theta_e}{2}, \tag{A2}$$

$$v_{TT} = -\frac{Q^2}{2q^2}, \tag{A3}$$

$$v_{LT} = -\frac{Q^2}{\sqrt{2}q^2}\sqrt{\frac{Q^2}{q^2} + \tan^2\frac{\theta_e}{2}}, \tag{A4}$$

$$v_{LT'} = -\frac{Q^2}{\sqrt{2}q^2}\tan\frac{\theta_e}{2}, \tag{A5}$$

$$v_{T'} = \tan\frac{\theta_e}{2}\sqrt{\frac{Q^2}{q^2} + \tan^2\frac{\theta_e}{2}}. \tag{A6}$$

The response functions in the xyz frame are given by

$$\begin{aligned} R_L(D) &= R_L^{(I)}(D) = W^{00}(D), \\ R_T(D) &= R_T^{(I)} = W^{11}(D) + W^{22}(D), \\ R_{TT}(D) &= R_{TT}^{(I)}(D)\cos 2\phi + R_{TT}^{(II)}(D)\sin 2\phi, \\ R_{LT}(D) &= R_{LT}^{(I)}(D)\cos\phi + R_{LT}^{(II)}(D)\sin\phi, \\ R_{LT'}(D) &= R_{LT'}^{(I)}(D)\sin\phi + R_{LT'}^{(II)}(D)\cos\phi, \\ R_{T'}(D) &= R_{T'}^{(II)} = -2\Re(W^{12}(D)), \end{aligned} \tag{A7}$$

where

$$\begin{aligned} R_{TT}^{(I)}(D)\cos 2\phi &= W^{22}(D) - W^{11}(D), \\ R_{TT}^{(II)}(D)\sin 2\phi &= 2\Re(W^{12}(D)), \\ R_{LT}^{(I)}(D)\sin\phi &= 2\sqrt{2}\Re(W^{01}(D)), \\ R_{LT}^{(II)}(D)\cos\phi &= -2\sqrt{2}\Re(W^{02}(D)), \\ R_{LT'}^{(I)}(D)\sin\phi &= -2\sqrt{2}\Im(W^{01}(D)), \\ R_{LT'}^{(II)}(D)\cos\phi &= -2\sqrt{2}\Im(W^{02}(D)). \end{aligned} \tag{A8}$$

APPENDIX B: ROTATIONS

The form of the differential cross section given by Eq. (67) assumes that the deuteron is polarized relative the direction of the momentum transfer $\mathbf{q}$. As a practical matter, polarized deuteron targets are generally polarized along the direction of the incident beam parallel to $\mathbf{k}$. Re-expressing the cross section for polarization to lie along the beam simply requires that the density matrix be rotated from $\boldsymbol{q}$ to $\boldsymbol{k}$. This involves a rotation of the density matrix through an angle θ_{kq}, where

$$\theta_{kq} = \cos^{-1}\frac{|\boldsymbol{k}| - |\boldsymbol{k}'|\cos\theta_l}{|\boldsymbol{q}|}. \tag{B1}$$

The components of the density matrix are given by the matrix elements of the density matrix operator $\hat{\rho}^d$ as

$$\rho^D_{\lambda_d\lambda'_d} = \langle\lambda_d|\hat{\rho}^D|\lambda'_d\rangle. \tag{B2}$$

The density matrix operator $\hat{\tilde{\rho}}$ Aligned along $\boldsymbol{k}$ is obtained by a right handed rotation about the y axis through the angle θ_{kq} which can be written as

$$\hat{\tilde{\rho}}^D = \hat{R}(\hat{y},\theta_{kq})\rho^D\hat{R}^{-1}(\hat{y},\theta_{kq}). \tag{B3}$$

The inverse of this expression is

$$\hat{\rho}^D = \hat{R}^{-1}(\hat{y},\theta_{kq})\hat{\tilde{\rho}}^D\hat{R}(\hat{y},\theta_{kq}) = \hat{R}(\hat{y},-\theta_{kq})\hat{\tilde{\rho}}^D\hat{R}(\hat{y},\theta_{kq}). \tag{B4}$$

So the matrix element of density operator is related to the rotated operator by

$$\rho^D_{\lambda_d\lambda'_d} = \sum_{\lambda''_d\lambda'''_d} d^1_{\lambda_d\lambda''_d}(-\theta_{kq})\tilde{\rho}^D_{\lambda''_d\lambda'''_d}d^1_{\lambda'''_d\lambda'_d}(\theta_{kq}). \tag{B5}$$

The density matrix can be related the density matrix polarized relative to $\boldsymbol{k}$ can be obtained using Eq. (B5), where

$$\boldsymbol{d}^1(\theta) = \begin{pmatrix} \frac{1}{2}(1+\cos\theta) & -\frac{1}{\sqrt{2}}\sin\theta & \frac{1}{2}(1-\cos\theta) \\ \frac{1}{\sqrt{2}}\sin\theta & \cos\theta & -\frac{1}{\sqrt{2}}\sin\theta \\ \frac{1}{2}(1-\cos\theta) & \frac{1}{\sqrt{2}}\sin\theta & \frac{1}{2}(1+\cos\theta) \end{pmatrix} \tag{B6}$$

and representing the rotated density matrix by

$$\tilde{\boldsymbol{\rho}}^D = \frac{1}{3}\left[\sum_{J=0}^{2}\tilde{T}_{J0}\boldsymbol{\tau}_{J0} + \sum_{J=1}^{2}\sum_{M=1}^{J}\left(\Re(\tilde{T}_{JM})\boldsymbol{\tau}^{\Re}_{JM} + \Im(\tilde{T}_{JM})\boldsymbol{\tau}^{\Im}_{JM}\right)\right]. \tag{B7}$$

The polarization coefficients can then be extracted using the properties of the matrices (36) to give the polarization coefficients in terms of the rotated polarization coefficients yielding

$$\begin{aligned} T_{10} &= \cos\theta_{kq}\widetilde{T}_{10} - \sqrt{2}\sin\theta_{kq}\Re\widetilde{T}_{11}, \\ \Re(T_{11}) &= \frac{1}{\sqrt{2}}\sin\theta_{kq}\widetilde{T}_{10} + \cos\theta_{kq}\Re\widetilde{T}_{11}, \\ \Im(T_{11}) &= \Im\widetilde{T}_{11}, \\ T_{20} &= \frac{1}{4}(1+3\cos 2\theta_{kq})\widetilde{T}_{20} - \sqrt{\frac{3}{2}}\sin 2\theta_{kq}\Re\widetilde{T}_{21} \\ &\quad + \sqrt{\frac{3}{8}}(1-\cos 2\theta_{kq})\Re\widetilde{T}_{22}, \end{aligned}$$

$$\Re(T_{21}) = \sqrt{\frac{3}{8}}\sin 2\theta_{kq}\widetilde{T}_{20} + \cos 2\theta_{kq}\Re\widetilde{T}_{21} - \frac{1}{2}\sin 2\theta_{kq}\Re\widetilde{T}_{22},$$
$$\Im(T_{21}) = \cos\theta_{kq}\Im\widetilde{T}_{21} - \sin\theta_{kq}\Im\widetilde{T}_{22},$$
$$\Re(T_{22}) = \sqrt{\frac{3}{32}}(1-\cos 2\theta_{kq})\widetilde{T}_{20} + \frac{1}{2}\sin 2\theta_{kq}\Re\widetilde{T}_{21} + \frac{1}{4}(3+\cos 2\theta_{kq})\Re\widetilde{T}_{22},$$
$$\Im(T_{22}) = \sin\theta_{kq}\Im\widetilde{T}_{21} + \cos\theta_{kq}\Im\widetilde{T}_{22}. \tag{B8}$$

APPENDIX C: SINGLE NUCLEON OFF-SHELL RESPONSE FUNCTION

The effective single-nucleon off-shell response functions are given by

$$\begin{aligned} r_L^{(I)} = \frac{1}{64\pi m_N^4}\{ & -4F_1^2(Q^2)m_N^2Q^2 - 8F_1(Q^2)F_2(Q^2)m_N^2(\nu^2+Q^2) + 4E_p^2\big(4F_1^2(Q^2)m_N^2 \\ & + F_2^2(Q^2)Q^2\big) + 4E_p\nu\big(4F_1^2(Q^2)m_N^2 + F_2^2(Q^2)Q^2\big) + F_2^2(Q^2)\big(\nu^2Q^2 - 4m_N^2(\nu^2+Q^2)\big) \\ & - 2\delta(2E_p+\nu)\big(-4F_1^2(Q^2)m_N^2 + F_2^2(Q^2)(2E_p\nu+\nu^2-Q^2)\big) \\ & + \delta^2\big[-4E_p^2F_2^2(Q^2) + 4F_1^2(Q^2)m_N^2 - 12E_pF_2^2(Q^2)\nu + F_2^2(Q^2)(-5\nu^2+Q^2)\big] - 4\delta^3F_2^2(Q^2)(E_p+\nu) - \delta^4F_2^2(Q^2)\}, \end{aligned} \tag{C1}$$

$$\begin{aligned} r_T^{(I)} = \frac{1}{64\pi m_N^4}\{ & 4\big[4F_1(Q^2)F_2(Q^2)m_N^2Q^2 + F_2^2(Q^2)\big(2m_N^2+p_\perp^2\big)Q^2 + 2F_1^2(Q^2)m_N^2(2p_\perp^2+Q^2)\big] \\ & - 16\delta F_1(Q^2)(F_1(Q^2)+F_2(Q^2))m_N^2\nu + \delta^2\big(8E_p^2F_2^2(Q^2) - 8F_1^2(Q^2)m_N^2 + 8E_pF_2^2(Q^2)\nu \\ & - 2F_2^2(Q^2)Q^2\big) + 4\delta^3F_2^2(Q^2)(2E_p+\nu) + 2\delta^4F_2^2(Q^2)\}, \end{aligned} \tag{C2}$$

$$r_{TT}^{(I)} = \frac{-4p_\perp^2\big(4F_1^2(Q^2)m_N^2 + F_2^2(Q^2)Q^2\big)}{64\pi m_N^4}, \tag{C3}$$

$$\begin{aligned} r_{LT}^{(I)} = \frac{1}{64\pi m_N^4}4\sqrt{2}\{ & (2E_p+\nu)p_\perp\big(4F_1^2(Q^2)m_N^2 + F_2^2(Q^2)Q^2\big) \\ & + \delta p_\perp\big[4F_1^2(Q^2)m_N^2 + F_2^2(Q^2)(-2E_p\nu-\nu^2+Q^2)\big] - \delta^2F_2^2(Q^2)\nu p_\perp\}, \end{aligned} \tag{C4}$$

$$\begin{aligned} r_{LT'}^{(II)} = \frac{\sqrt{2}p_\perp q}{16\pi m_N^4 p}\big[& E_p^2F_2^2(Q^2)\nu - 4E_pF_1(Q^2)m_N^2(F_1(Q^2)+F_2(Q^2)) \\ & + F_2(Q^2)\nu\big(2F_1(Q^2)m_N^2 + F_2(Q^2)\big)\big(m_N^2-p^2\big) + \delta E_pF_2^2(Q^2)(2E_p+\nu) + \delta^2E_pF_2^2(Q^2)\big], \end{aligned} \tag{C5}$$

$$\begin{aligned} r_{T'}^{(II)} = \frac{1}{16\pi m_N^4 p}\big[& \big(E_p^2p_\parallel\big(4F_1^2(Q^2)m_N^2 + F_2^2(Q^2)Q^2\big) + 4E_pF_1(Q^2)m_N^2\nu p_\parallel(F_1(Q^2)+F_2(Q^2)) \\ & - 4F_1^2(Q^2)m_N^2\big(m_N^2p_\parallel + p^2(p_\parallel+q)\big) + 2F_1(Q^2)F_2(Q^2)m_N^2(p_\parallel Q^2 - 2p^2q) \\ & + F_2^2(Q^2)p_\parallel Q^2\big(m_N^2-p^2\big)\big) + \delta E_p\big(F_2^2(Q^2)(-2E_p\nu p_\parallel + 2p^2q + p_\parallel Q^2\big) \\ & + 4F_1^2(Q^2)m_N^2p_\parallel + 4F_1(Q^2)F_2(Q^2)m_N^2p_\parallel\big) + \delta^2F_2(Q^2)\big(-E_pF_2(Q^2)\nu p_\parallel + 2F_1(Q^2)m_N^2p_\parallel + F_2(Q^2)p^2q\big)\big], \end{aligned} \tag{C6}$$

where $p = p_m$, $p_\perp = p\sin\theta_m$, and $p_\parallel = p\cos\theta_m$.

[1] J. L. Friar, Ann. Phys. (NY) **104**, 380 (1977).
[2] J. L. Friar, Phys. Rev. C **20**, 325 (1979).
[3] R. D. Amado, M. P. Locher, and M. Simonius, Phys. Rev. C **17**, 403 (1978).
[4] R. D. Amado, *Proceedings of the Few Body Problems in Nuclear and Particle Physics*, edited by R. J. Slobodrian *et al.* (Quebec, Canada, Les Presses de l'Universite Laval, 1974), pp. 2–11.
[5] T. De Forest, Nucl. Phys. A **392**, 232 (1983).
[6] G. van der Steenhoven, International Symposium on Mesons and Light Nuclei V Prague, Czechoslovakia, September 1–6, 1991 [Few Body Syst. Suppl. **5**, 17 (1992)].
[7] G. van der Steenhoven, M. van der Schaar, H. Arenhövel, H. P. Blok, E. Hummel, E. Jans, L. Lapikas, J. A. Tjon, and P. K. A. de Witt Huberts, *Proceedings of the 4th Conference on the Intersections between Particle and Nuclear Physics, Tucson, AZ*, May 23–29 (1991); AIP Conf. Proc. No. 243 (AIP, New York, 1992), p. 793.
[8] M. van der Schaar *et al.*, Phys. Rev. Lett. **66**, 2855 (1991).
[9] M. van der Schaar *et al.*, Phys. Rev. Lett. **68**, 776 (1992).
[10] W.-J. Kasdorp *et al.*, Phys. Lett. B **393**, 42 (1997).
[11] W. J. Kasdorp *et al.*, Few Body Syst. **25**, 115 (1998).

[12] A. Bussiere, J. Mougey, D. Royer, D. Tarnowski, S. Turck-Chieze, M. Bernheim, S. Frullani, G. P. Capitani, E. De Sanctis, and E. Jans, Nucl. Phys. A **365**, 349 (1981).
[13] S. Turck-Chieze *et al.*, Phys. Lett. B **142**, 145 (1984).
[14] J. E. Ducret *et al.*, Nucl. Phys. **A553**, 697C (1993).
[15] J. E. Ducret *et al.*, Phys. Rev. C **49**, 1783 (1994).
[16] Z.-L. Zhou *et al.*, Phys. Rev. Lett. **82**, 687 (1999).
[17] Z.-L. Zhou *et al.* (The MIT-Bates OOPS Collaboration), Phys. Rev. Lett. **87**, 172301 (2001).
[18] P. Ulmer, K. Aniol, H. Arenhovel, J. Chen, E. Chudakov *et al.*, Phys. Rev. Lett. **89**, 062301 (2002).
[19] B. Hu *et al.*, Phys. Rev. C **73**, 064004 (2006).
[20] W. U. Boeglin *et al.*, Phys. Rev. C **78**, 054001 (2008).
[21] W. U. Boeglin, L. Coman, P. Ambrozewicz, K. Aniol, J. Arrington, G. Batigne, P. Bosted, A. Camsonne, G. Chang, J. P. Chen, S. Choi, A. Deur, M. Epstein, J. M. Finn, S. Frullani, C. Furget, F. Garibaldi, O. Gayou, R. Gilman, O. Hansen, D. Hayes, D. W. Higinbotham, W. Hinton, C. Hyde, H. Ibrahim, C. W. de Jager, X. Jiang, M. K. Jones, L. J. Kaufman, A. Klein, S. Kox, L. Kramer, G. Kumbartzki, J. M. Laget, J. LeRose, R. Lindgren, D. J. Margaziotis, P. Markowitz, K. McCormick, Z. Meziani, R. Michaels, B. Milbrath, J. Mitchell, P. Monaghan, M. Moteabbed, P. Moussiegt, R. Nasseripour, K. Paschke, C. Perdrisat, E. Piasetzky, V. Punjabi, I. A. Qattan, G. Quéméner, R. D. Ransome, B. Raue, J. S. Réal, J. Reinhold, B. Reitz, R. Roché, M. Roedelbronn, A. Saha, K. Slifer, P. Solvignon, V. Sulkosky, P. E. Ulmer, E. Voutier, L. B. Weinstein, B. Wojtsekhowski, and M. Zeier (for the Hall A Collaboration), Phys. Rev. Lett. **107**, 262501 (2011).
[22] H. Arenhovel and K. M. Schmitt, Few Body Syst. **8**, 77 (1990).
[23] T. Wilbois, G. Beck, and H. Arenhovel, Few Body Syst. **15**, 39 (1993).
[24] H. Arenhovel, *Workshop on Electronuclear Physics with Internal Targets and the BLAST Detector Tempe, Arizona, March 19–20* (1992), pp. 16–42.
[25] J. Adam, H. Goller, and H. Arenhovel, Phys. Rev. C **48**, 370 (1993).
[26] H. Arenhovel, W. Leidemann, and E. L. Tomusiak, Phys. Rev. C **52**, 1232 (1995).
[27] H. Arenhovel, W. Leidemann, and E. L. Tomusiak, Nucl. Phys. A **641**, 517 (1998).
[28] H. Arenhovel, W. Leidemann, and E. L. Tomusiak, Few Body Syst. **28**, 147 (2000).
[29] H. Arenhovel, Int. J. Mod. Phys. **E18**, 1226 (2009).
[30] A. Bianconi, S. Jeschonnek, N. N. Nikolaev, and B. G. Zakharov, Phys. Lett. B **343**, 13 (1995).
[31] A. Bianconi, S. Jeschonnek, N. N. Nikolaev, and B. G. Zakharov, Nucl. Phys. A **608**, 437 (1996); Erratum: **616**, 680 (1997).
[32] A. Bianconi, S. Jeschonnek, N. N. Nikolaev, and B. G. Zakharov, Phys. Lett. B **363**, 217 (1995).
[33] S. Jeschonnek and J. W. Van Orden, Phys. Rev. C **78**, 014007 (2008).
[34] S. Jeschonnek and J. W. Van Orden, Phys. Rev. C **80**, 054001 (2009).
[35] S. Jeschonnek, Phys. Rev. C **63**, 034609 (2001).
[36] J. Adam, Jr., F. Gross, S. Jeschonnek, P. Ulmer, and J. W. Van Orden, Phys. Rev. C **66**, 044003 (2002).
[37] J. Ryckebusch, S. Janssen, W. Van Nespen, and D. Debruyne, Phys. Rev. C **61**, 021603(R) (2000).
[38] J. Ryckebusch, W. Cosyn, and M. Vanhalst, J. Phys. G **42**, 055104 (2015).
[39] W. Cosyn and M. Sargsian, Phys. Rev. C **84**, 014601 (2011).
[40] W. Cosyn, W. Melnitchouk, and M. Sargsian, Phys. Rev. C **89**, 014612 (2014).
[41] W. Cosyn and M. Sargsian, J. Phys. Conf. Ser. **543**, 012006 (2014).
[42] W. Cosyn, V. Guzey, D. W. Higinbotham, C. Hyde, S. Kuhn, P. Nadel-Turonski, K. Park, M. Sargsian, M. Strikman, and C. Weiss, J. Phys. Conf. Ser. **543**, 012007 (2014).
[43] W. Cosyn, V. Guzey, M. Sargsian, M. Strikman, and C. Weiss, EPJ Web Conf. **112**, 01022 (2016).
[44] W. Cosyn, M. Sargsian, and C. Weiss, *Proceedings of the 24th International Workshop on Deep-Inelastic Scattering and Related Subjects (DIS 2016): Hamburg, Germany, April 11–15, 2016* [PoS **DIS2016**, 210 (2016)].
[45] W. Cosyn and M. Sargsian, EPJ Web Conf. **112**, 03001 (2016).
[46] K. Slifer, J.-P. Chen, O. R. Aramayo, D. Keller, N. Kalantarians, E. Long *et al.*, The Deuteron Tensor Structure Function b1, Jefferson Lab conditionally approved experiment no. E12-13-011 (2013) (unpublished).
[47] E. Long, K. Slifer, P. Solvignon, D. Day, D. Keller, D. Higinbotham *et al.*, Measurements of the Quasi-Elastic and Elastic Deuteron Tensor Asymmetries, Jefferson Lab conditionally approved experiment no. C12-15-005 (2015) (unpublished).
[48] A. S. Raskin and T. W. Donnelly, Ann. Phys. (NY) **191**, 78 (1989) Erratum: **197**, 202 (1990).
[49] V. Dmitrasinovic and F. Gross, Phys. Rev. C **40**, 2479 (1989) Erratum: **43**, 1495 (1991).
[50] L. L. Frankfurt and M. I. Strikman, Nucl. Phys. A **405**, 557 (1983).
[51] A. Bianconi, S. Jeschonnek, N. N. Nikolaev, and B. G. Zakharov, Phys. Rev. C **53**, 576 (1996).
[52] W. P. Ford, S. Jeschonnek, and J. W. Van Orden, Phys. Rev. C **90**, 064006 (2014).
[53] W. P. Ford and J. W. Van Orden, Phys. Rev. C **87**, 014004 (2013).
[54] W. P. Ford, S. Jeschonnek, and J. W. Van Orden, Phys. Rev. C **87**, 054006 (2013).
[55] W. P. Ford (2013), arXiv:1310.0871 [nucl-th].
[56] SAID, http://gwdac.phys.gwu.edu/, accessed: 2012-09-21.
[57] R. A. Arndt, W. J. Briscoe, I. I. Strakovsky, and R. L. Workman, Phys. Rev. C **76**, 025209 (2007).
[58] R. A. Arndt, I. I. Strakovsky, and R. L. Workman, Phys. Rev. C **62**, 034005 (2000).
[59] E. L. Lomon, Phys. Rev. C **66**, 045501 (2002).
[60] E. L. Lomon (2006), arXiv:nucl-th/0609020 [nucl-th].
[61] J. Arrington, W. Melnitchouk, and J. A. Tjon, Phys. Rev. C **76**, 035205 (2007).
[62] P. Mergell, U.-G. Meißner, and D. Drechsel, Nucl. Phys. A **596**, 367 (1996).
[63] F. Gross, J. W. Van Orden, and K. Holinde, Phys. Rev. C **45**, 2094 (1992).
[64] F. Gross and A. Stadler, Few Body Syst. **44**, 295 (2008).
[65] R. B. Wiringa, V. G. J. Stoks, and R. Schiavilla, Phys. Rev. C **51**, 38 (1995).
[66] R. Machleidt, Phys. Rev. C **63**, 024001 (2001).
[67] V. G. J. Stoks, R. A. M. Klomp, C. P. F. Terheggen, and J. J. de Swart, Phys. Rev. C **49**, 2950 (1994).